Thermal Science & Engineering Vol. 10 No.6 (2002)

Molecular Scale Aspects of Liquid Contact on a Solid Surface*

Shigeo MARUYAMA†, Tatsuto KIMURA† and Ming-Chang LU‡

Abstract

Molecular dynamics simulations related to the contact structure of liquid droplet on a solid surface are compared for a simple Lennard-Jones fluid system and a practical water-on-platinum system. The contact angle for the Lennard-Jones system seems to be simply scaled with the potential energy parameter between liquid and solid, even though the layered liquid structure near the surface gives some complexity. On the other hand, a water droplet in contact with a platinum surface shows quite intrigue results. The water droplet gives a finite contact angle on the absorbed monolayer water film. The contact angle is determined by the surface energy between this monolayer water film and bulk liquid water. The dependence of contact angle on the platinum crystal lattice structure is explained by the structure of this monolayer water film.

Key Words: *Molecular Dynamics Method, Contact Angle, Wetting, Lennard-Jones, Water, Platinum*

Nomenclature

a : potential parameter of S-H potential
b : potential parameter of S-H potential
c : potential parameter of S-H potential
H_c : height of fitting circle center
N : number of molecules
q : electrical charge
$R_{1/2}$: radius of fitting circle
R_0 : nearest neighbor distance of solid crystal
r : distance

Greek Symbols
α : potential parameter of Z-P potential
Δr : liquid extension parameter
ε : potential parameter of Lennard-Jones potential
γ : surface energy
ϕ : potential function
θ : contact angle
θ_∞ : asymptotic contact angle for macroscopic system
ρ : length of the projection of the distance vector onto the surface plane
σ : potential parameter of Lennard-Jones potential

Subscripts
an : anisotropic
cond : conductance
H : hydrogen
H_2O : water molecule
INT : interaction between liquid and solid molecules
L : liquid
LG : liquid-gas interface
isr : isotropic
O : oxygen
Pt : platinum
SG : solid-gas interface
SL : solid-liquid interface
surf : surface

1 Introduction

Solid-liquid-vapor interaction phenomena or simply contact phenomena of liquid to the solid surface have a very important role in phase-change heat transfer. Except for the direct contact heat transfer, most practical phase-change heat-transfer problems involve the solid surface as a heater or a condenser. The importance of the liquid wettability to the surface is apparent in a dropwise condensation, high-heat-flux boiling heat transfer and capillary liquid film evaporators. The mechanical and thermodynamic treatments of the traditional macroscopic approach had difficulties in the treatment of the line of three-phase contact. The contact line is the singular point

* Received: October 18, 2002, Editor: Mamoru OZAWA
† Department of Mechanical Engineering, The University of Tokyo (7-3-1 Hongo, Bunkyo-ku, Tokyo 113-8656, JAPAN)
‡ Current Address: Energy & Research Lab., Industrial Technology Research Institute (Bldg. 64, 195-6, Sec. 4, Chung Hsing Rd., Chutung, Hsinchu, TAIWAN)

in the macroscopic sense, since the non-slip condition of fluid dynamics, i.e. $U = V = 0$ at the surface, simply denies the movement of the contact line. The curious "monolayer liquid film" considered in some macroscopic theories of heat transfer should be examined from the molecular scale considerations. The molecular dynamics method is one of the most powerful techniques for this purpose [1], even though the simulations of macroscopic phenomena are not easy due to the severe limitations of current computational power.

Recently, the liquid-solid contact phenomena for nanoscale system are also very important in some nanotechnology applications such as the wetting of catalyst metal in a fuel cell electrode. The use of molecular dynamics simulations is much more straightforward for such nanoscale system. Here, again, it is practically important to compare such nanoscale phenomena with macroscopic phenomena, because an analogy to the larger system is often an important strategy in order to understand a phenomenon. An important feature intrinsic to a nanoscale system is usually found through the rational comparison with a macroscopic system.

Many molecular dynamics simulations in heat transfer adopt the Lennard-Jones fluid as the test liquid, even though this potential is best used only for rare gas molecules such as Ar and Xe. In addition to its simplicity and well-established phase diagram, this potential is the basic component representing the van der Waals potential. Employing this Lennard-Jones fluid combined with the artificial solid surface, we have been studying the liquid droplet [2], the liquid contact on solid surface [3-5], nucleation of liquid droplet [6,7], nucleation of vapor bubble [8,9], and thermal boundary resistance in liquid-solid interface [10]. The liquid-solid contact with this simple molecule system results the interesting layered liquid structure near the surface. However, the contact angle, or the over-all shape of the liquid, is roughly explained by the analogy with Young's equation.

Recently, we have moved to the more practical combinations such as a water droplet on a platinum surface [11, 12]. Because a water molecule has the permanent dipole moment and makes the hydrogen bond, the contact phenomena are drastically different from the simple Lennard-Jones fluid. The water droplet exhibits a finite contact angle on the absorbed monolayer water film. The contact angle is determined by the surface energy between this monolayer water film and bulk liquid water film. The dependence of contact angle on the platinum crystal lattice orientation is explained by the structure of this monolayer water film.

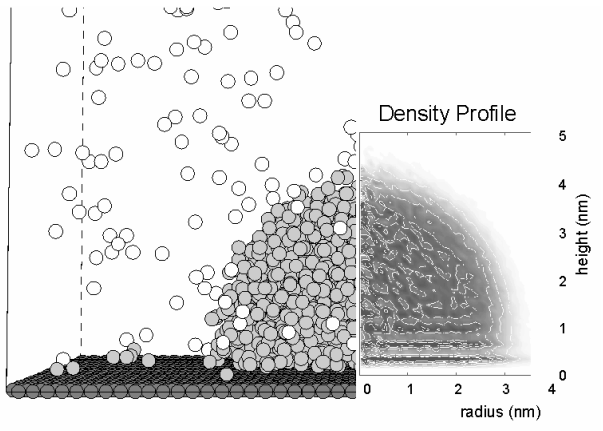

Fig. 1 A snapshot of a liquid droplet on solid surface compared with the two-dimensional density profile.

2 A Lennard-Jones Droplet on a Solid Surface [3-5]

The calculation region had periodic boundaries for four side surfaces and a mirror boundary (or a hard wall boundary) for the top surface as in Fig. 1 [3-5]. The bottom surface was expressed by harmonic molecules. The liquid droplet and the vapor consisted of Lennard-Jones molecules with the interaction potential expressed as

$$\phi(r) = 4\varepsilon\left\{\left(\frac{\sigma}{r}\right)^{12} - \left(\frac{\sigma}{r}\right)^{6}\right\} \tag{1}$$

with $\sigma = 3.40$ Å, $\varepsilon = 1.67 \times 10^{-21}$ J, and $m = 6.63 \times 10^{-26}$ kg for argon.

The potential between argon and solid molecule was also represented by the Lennard-Jones potential function with variable energy scale parameter ε_{INT}. The length scale of the interaction potential σ_{INT} was kept constant. Even though the harmonic potential parameters of 3-layers of solid surface (mass, spring constant, lattice spacing) were employed from platinum, this metal surface was an artificial model surface.

The effect of the interaction potential on the shape of the liquid droplet is shown in Fig. 2. Here, the strength of interaction potential ε_{INT} are in Table 1 with 1024 argon molecules at 100 K. With increase in the strength of the interaction potential between the surface molecule and argon, more wetting shape was observed. Furthermore, with stronger interaction potential, the

Table 1 Calculation conditions.

		Droplet		Bubble	
	ε^*_{SURF}	ε_{INT} [10^{-21}J]	θ [deg]	ε_{INT} [10^{-21}J]	θ [deg]
E0	0.73	0.228	-	-	-
E1	1.29	0.404	135	-	-
E2	1.86	0.581	110	0.527	101
E3	2.43	0.758	79	0.688	69
E4	2.99	0.935	49	0.848	23
E5	3.56	1.112	-	1.009	-

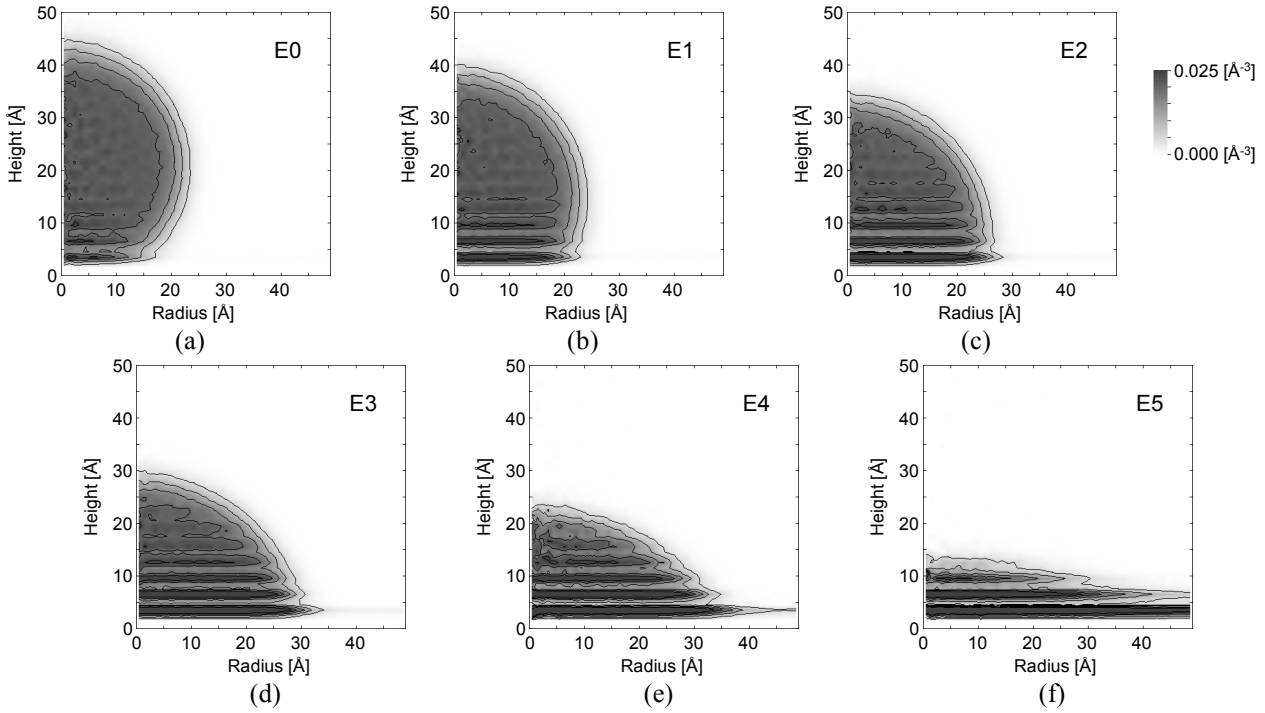

Fig. 2 Two dimensional density distributions for a Lennard-Jones droplet.

spread of the first layer of liquid film was much more pronounced. The layered structure near the surface was commonly observed for liquid-solid interfaces and explained as due to the solvation force [13].

Except for the two or three liquid layers near the surface, the averaged shape of the liquid droplet was close to the semi-spherical. In order to measure the 'contact angle', we fit a circle to a density contour disregarding the two layers of liquid near the solid surface. Controversially enough, the cosine of measured contact angle or the average shape of the droplet far from the surface was linearly dependent on the strength of the surface potential as shown in Fig. 3. Comparing simulations with different interaction length parameter σ_{INT} and different configuration of the solid surface such as one-dimensional function, one layer of fixed molecules, and three layers of harmonic molecules, we have proposed the effective integrated potential energy parameter ε_{SURF}, which correlates directly to the contact angle [4].

$$\varepsilon_{SUFR} = (4\sqrt{3}\pi/5)(\sigma_{INT}{}^2/R_0{}^2)\varepsilon_{INT}, \quad (2)$$

which is the energy depth of the integrated surface potential.

For the macroscopic contact, the well-known Young's equation relates the contact angle to the balance of surface energies as.

$$\cos\theta = \frac{\gamma_{SG} - \gamma_{SL}}{\gamma_{LG}} \quad (3)$$

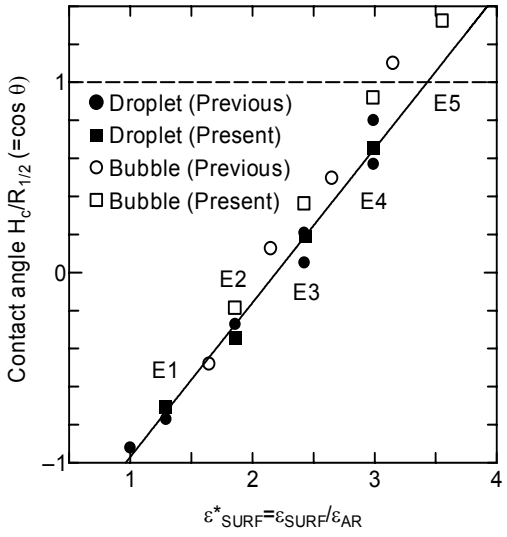

Fig. 3 Dependence of contact angle on the integrated depth of surface potential ε_{SURF}.

where γ_{SG}, γ_{SL} and γ_{LG} are surface energies between solid-gas, solid-liquid, and liquid-gas, respectively.

As we change the energy parameter between liquid and solid molecules, γ_{LG} is kept constant and γ_{SG} does not change much compared with γ_{SL} because the vapor density is much lower compared with liquid density. With increase in ε_{SURF}, γ_{SL} should decrease almost proportionally because of the gain in potential energy in liquid-solid interface. Then, (γ_{SG} - γ_{SL}) should increase and the Young's equation predicts the increase in $\cos\theta$.

Hence, the linear relation in Fig. 3 can be explained by the analogy with Young's equation.

Since the thickness and the extension of the layered structure near the surface are scaled with the molecule diameter (only up to about 5 molecular layers), the importance of this structure vanishes for large enough liquid droplet except for the modification of the liquid-solid surface energy γ_{LS}. The size dependence of the contact angle is shown in Fig. 4. By using the one-dimensional potential to represent the surface, up to N = 32000 system was calculated for the interaction potential parameters nearly equivalent to E4 in table 1. With increase in number of liquid molecules N_L of a droplet, the gradual decrease of $\cos\theta$ (increase of contact angle) was observed. We assume that the extended liquid layer near the surface is the primary factor of this size dependence. The extension of the liquid layer causes the increase of liquid-solid interface. Hence, this increase of the liquid-solid interface area is equivalent to the decrease of γ_{SL} (potential energy gain by liquid-solid interface reduces the surface energy), increase in (γ_{SG} - γ_{SL}), and hence, increase in $\cos\theta$ by Eq. (3). Assuming that the extension of the first liquid layer is constant irrespective to the size of the droplet, the following dependence of contact angle on the number of liquid molecules N_L can be derived.

$$\cos\theta = \cos\theta_\infty \frac{\left(N_L^{1/3} + \Delta r\right)^2}{N_L^{2/3}} \tag{4}$$

where θ_∞ is an asymptotic contact angle for macroscopic system, $N_L^{1/3}$ is proportional to the radius of the liquid-solid contact surface, and Δr is the parameter related to the extension of the interface. The solid line in Fig. 4 is the least-square fit with Eq. (4): $\cos\theta_\infty = 0.35$, $\Delta r = 2.72$.

The opposite configuration of liquid and vapor, i.e. a vapor bubble in liquid, is realized for negative pressure simulations [8,9]. Two dimensional density distributions for three different interaction potentials compatible to Fig. 2 are summarized in Fig. 5. Here, 5488 argon molecules at 110 K were employed. The completely opposite situation of liquid and vapor is apparent, except for the layered liquid structure, which is always extending from liquid to vapor area in order to relax the liquid-solid surface energy γ_{LS}. The contact angles measured in the same manner as for the droplet are summarized in Fig. 3. Principally, the bubble cases obey the same straight line as droplets. However, the contact angle measured for the vapor bubble is slightly smaller ($\cos\theta$ is larger) for more wetting cases than E3. This may be due to the fact that the extended liquid layer near the surface has merged. Probably, the merged liquid layer should contribute to the certain increase in stability of the system or the decrease of γ_{SL}. Then, the decrease of γ_{SL} leads to the increase of $(\gamma_{SG} - \gamma_{SL})$, the increase in $\cos\theta$, and the decrease of the contact angle θ. One interesting point about the vapor bubble is that the first liquid layer completely covers the surface for the very wettable case of E5 in Fig. 5(d). The vapor bubble is not touching the

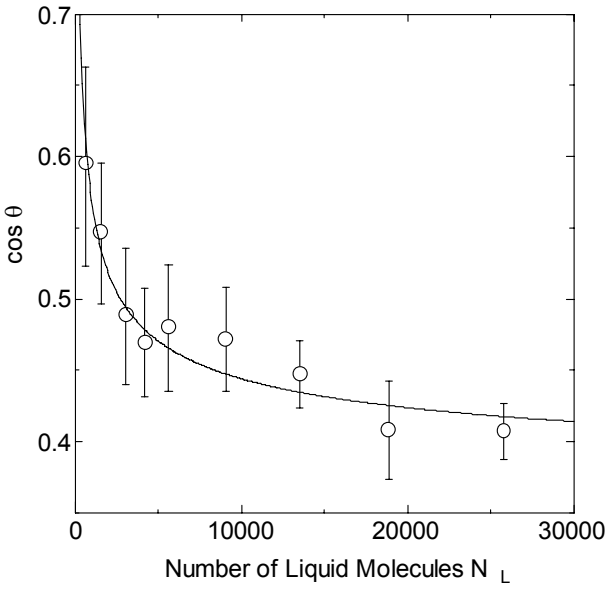

Fig. 4. Size dependence of contact angle.

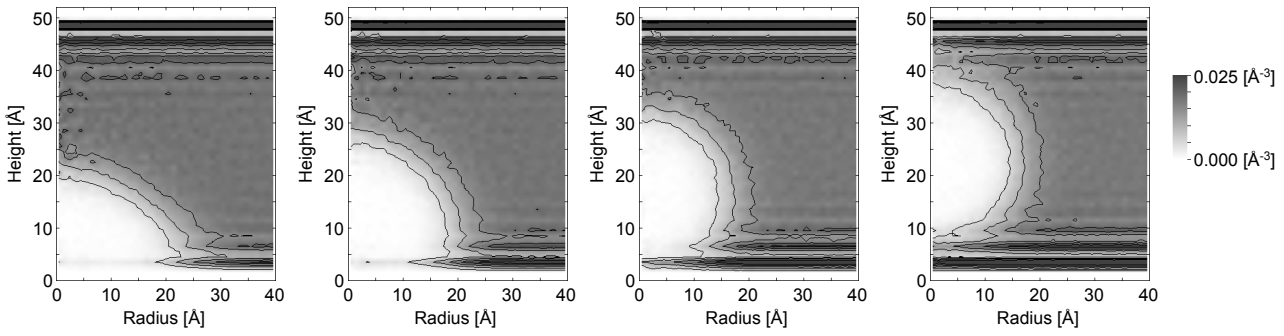

(a) E2 (b) E3 (c) E4 (d) E5

Fig. 5 Two dimensional density distributions for Lennard-Jones bubble.

surface, but it is certainly trapped in the surface through the surface energy balance. The conventional contact angle should be less than 0°. It was revealed that the $\cos\theta$ could be generalized to be $H_C/R_{1/2}$, to continuously express the dependency of the contact angle for the extremely wettable surface where H_C and $R_{1/2}$ were the center height and radius of the fitting circle [8, 9].

3 Water Droplet on Platinum Surface [11, 12]

Platinum surface was located at the bottom and mirror boundary condition at the top and periodic boundary conditions in 4 sides were employed. Water molecule was modeled with the well-known SPC/E model [14] and the platinum surface was represented by three layers of harmonic molecules. The phantom molecules [15, 16] were used beneath the layers of platinum surface in order to mimic the constant temperature heat bath.

Two different potential functions between water and platinum surface were employed. Both potential models were derived from the extended Hückel calculations between a water molecule and a platinum cluster [17]. One is the model developed by Spohr and Heinzinger in 1988 [18]. The potential function is described as follows.

$$\phi_{H_2O-Pt} = \phi_{O-Pt}(r_{OPt}, \rho_{OPt}) + \phi_{HPt}(r_{H_1Pt}) + \phi_{H-Pt}(r_{H_2Pt}) \quad (5)$$

$$\phi_{O-Pt} = [a_1 \exp(-b_1 r) - a_2 \exp(-b_2 r)] f(\rho) + a_3 \exp(-b_3 r)[1 - f(\rho)] \quad (6)$$

$$\phi_{H-Pt} = a_4 \exp(-b_4 r) \quad (7)$$

$$f(\rho) = \exp(-c\rho^2) \quad (8)$$

where $a_1 = 1.8942\times10^{-16}$ J, $b_1 = 11.004$ nm^{-1},
$a_2 = 1.8863\times10^{-16}$ J, $b_2 = 10.966$ nm^{-1},
$a_3 = 10^{-13}$ J, $b_3 = 53.568$ nm^{-1},
$a_4 = 1.742\times10^{-19}$ J, $b_4 = 12.777$ nm^{-1},
$c = 11.004$ nm^{-1}

Here, r is inter-atomic distance, and ρ is the length of the projection of the distance vector onto the surface plane. This potential has the minimum value when a water molecule sits on top of a platinum atom with the dipole moment directing upward.

The other potential model between water and platinum surface was developed by Zhu and Philpott in 1994 [19]. The potential function consists of water molecule-conduction electron potential, anisotropic short-range potential and isotropic short-range r^{-10} potential as follows.

$$\phi_{H_2O-surf} = \phi_{H2O-cond} + \phi_{an}(O;\mathbf{r}_O) + \phi_{isr}(O;\mathbf{r}_O) + \sum_H [\phi_{an}(H;\mathbf{r}_H) + \phi_{isr}(H;\mathbf{r}_H)] \quad (9)$$

$$\phi_{H2O-cond} = \sum_{l,k} \frac{q_l q_k}{2r_{lk}} \quad (10)$$

$$\phi_{an}(p;\mathbf{r}_p) = 4\varepsilon_{p-Pt} \sum_j \left[\left(\frac{\sigma_{p-Pt}^2}{(\alpha\rho_{pj})^2 + z_{pj}^2} \right)^6 \right.$$

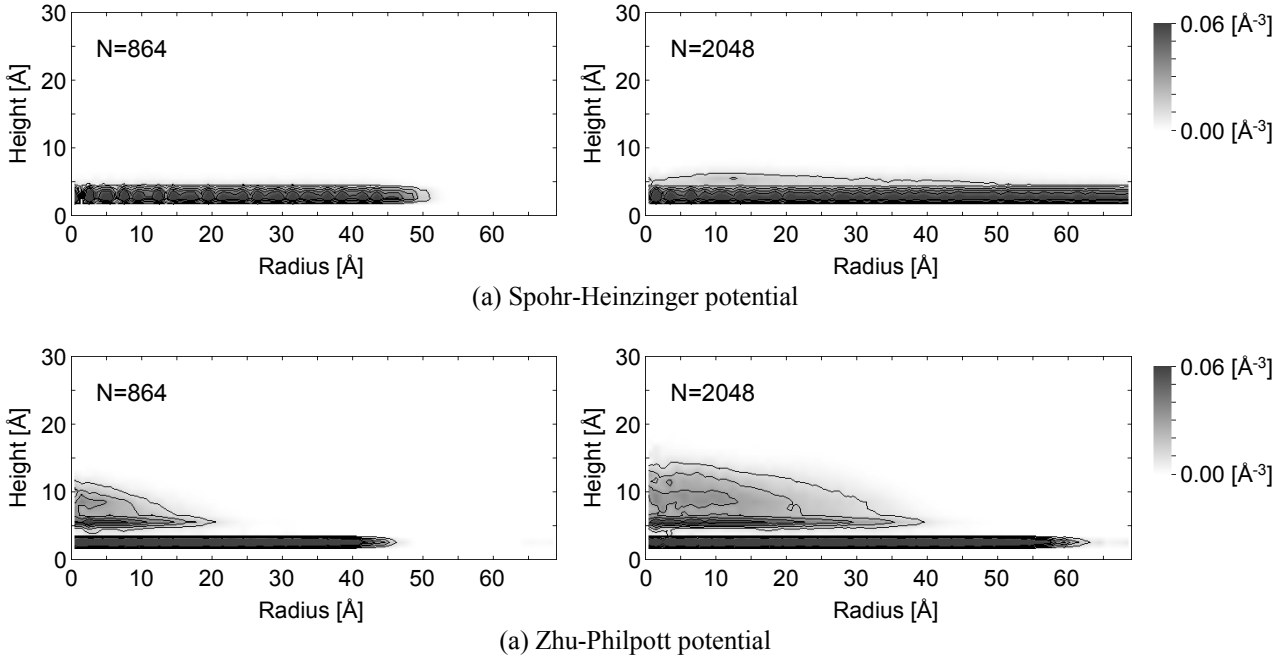

(a) Spohr-Heinzinger potential

(a) Zhu-Philpott potential

Fig. 6 Two-dimensional density profiles of water droplet on fcc (111) platinum surface.

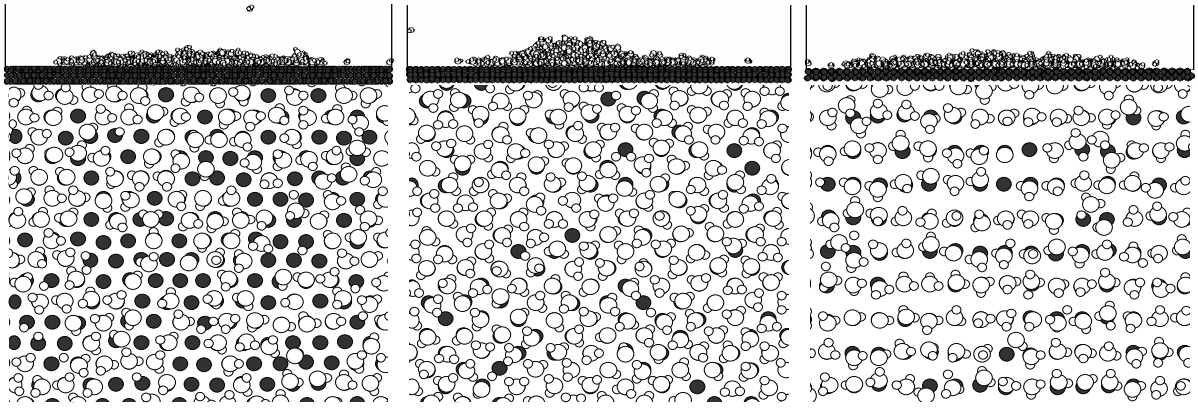

(a) fcc (111) (b) fcc (100) (c) fcc (110)

Fig.7 Snapshots of water droplet and the first layer (Spohr-Heinzinger potential).

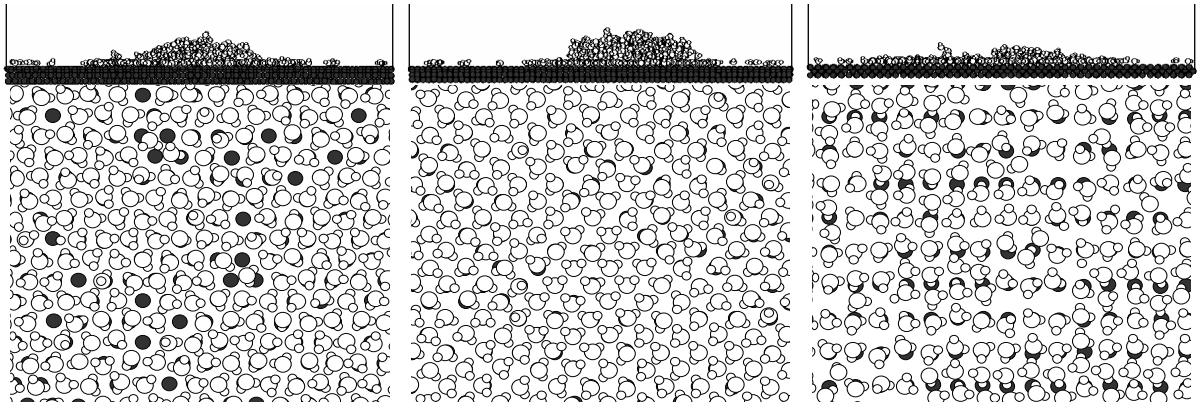

(a) fcc (111) (b) fcc (100) (c) fcc (110)

Fig.8 Snapshots of water droplet and the first layer (Zhu-Philpott potential).

$$-\left(\frac{\sigma_{p-\mathrm{Pt}}{}^{2}}{\left(\rho_{pj}/\alpha\right)^{2}+z_{pj}{}^{2}}\right)^{3}\Bigg] \quad (11)$$

$$\phi_{\mathrm{isr}}\left(p;\mathbf{r}_{p}\right)=-4\varepsilon_{p-\mathrm{Pt}}\sum_{j}\frac{c_{p-\mathrm{Pt}}\sigma_{p-\mathrm{Pt}}{}^{10}}{r_{pj}{}^{10}} \quad (12)$$

where

$\alpha = 0.8$

$\sigma_{\mathrm{O\text{-}Pt}} = 0.270$ nm, $\varepsilon_{\mathrm{O\text{-}Pt}} = 6.44\times10\text{-}21$ J, $c_{\mathrm{O\text{-}Pt}} = 1.28$

$\sigma_{\mathrm{H\text{-}Pt}} = 0.255$ nm, $\varepsilon_{\mathrm{H\text{-}Pt}} = 3.91\times10^{-21}$ J, $c_{\mathrm{H\text{-}Pt}} = 1.2$

Equation (10) represents Coulomb potential between point charge of water molecule and its image charge located at symmetrical position below the image plane. This potential also has the minimum value when a water molecule sits on top of a platinum atom, but the binding energy is stronger than the S-H potential.

As the initial condition, an ice crystal with 864 or 2048 molecules with the density of bulk water at 350 K was placed on the center of the platinum surface. For the initial 100 ps, simple velocity scaling was used for the temperature control. After this initial rough control, only the phantom heat bath was employed as the temperature control at 350K.

Fig. 6 shows the two-dimensional density distributions of the equilibrium water droplets on fcc (111) surface. In the case of S-H potential, the droplet finally spread to almost monolayer and only a few molecules stayed on the film. On the other hand, in the case of the Z-P potential, a liquid droplet with a contact angle on the monolayer was observed. This is the first realization of equilibrium droplet structure on the precursor film with molecular dynamics level calculation. Even though the existence of the precursor film is anticipated in wetting theories, the clear physical understanding of the three phase contact line has not been obtained. The simple relation obtained for the Lennard-Jones fluid is that the interface potential strength is proportional to the cosine of contact angle. This can be readily imagined by the analogy to the Young's equation. However, the stronger interaction in the Z-P potential now results the less wetting structure compared with the S-H potential. The reason for this apparently controversial result can be explained as follows. The monolayer is very dense and there is a gap between the monolayer and the droplet. The dense

monolayer repulses the other water molecules, so that the effective potential between a platinum surface and the droplet on the monolayer is weakened. Hence, the higher concentration of the monolayer leads to the larger contact angle (less wettable).

Fig. 7 and Fig. 8 show snapshots of the water droplet and its first layer on different surface lattice structures employing the S-H potential and the Z-P potential, respectively. The platinum surface atom site density is largest for (111), medium for (100) and smallest for (110). Water molecules almost completely cover platinum atoms for (100) and (110) but the surface atom density is too large for (111). Hence, the water molecular density of monolayer is the order of (100), (111), and (110) from largest. The order of the contact angle is the same: largest for (100), medium for (111), and smallest for (110). These trends are valid for both the S-H (weaker) and Z-P (stronger) potentials in Fig. 7 and 8. Hence, the explanation based on the monolayer density is confirmed.

4 Conclusions

Molecular dynamics simulations of liquid-solid contact phenomena are compared for a simple Lennard-Jones fluid system and a practical water-on-platinum system. For Lennard-Jones system, the contact angle can be explained by the macroscopic concept of surface energy balance, even though the layered structure of liquid near the solid wall makes the situation complicated. On the other hand, a water droplet in contact with a platinum surface shows quite intrigue results. The contact structure of the water droplet with a finite contact angle on the absorbed monolayer water film is realized for the first time with molecular dynamics simulation. The contact angle is determined by the surface energy between this monolayer water film and bulk liquid water. The dependence of contact angle on the platinum crystal lattice structure is explained by the structure of this monolayer water film.

References

[1] Maruyama, S., “Molecular Dynamics Method for Microscale Heat Transfer,” *Advances in Numerical Heat Transfer*, **2** (2000), 189-226.

[2] Maruyama, S., Matsumoto, S. and Ogita, A., "Surface Phenomena of Molecular Clusters by Molecular Dynamics Method," *Therm. Sci. Eng.*, **2**-1 (1994), 77-84.

[3] Matsumoto, S., Maruyama, S. and Saruwatari, H., "A Molecular Dynamics Simulation of a Liquid Droplet on a Solid Surface, " *Proc. ASME/JSME Therm. Eng. Conf.*, Maui, (1995), 557-562.

[4] Maruyama, S., Kinoshita, S. and Yamaguchi, Y., "A Molecular Dynamics Simulation of a Liquid Droplet on a Solid Surface (Part 2: Effect of Vibration of Solid Molecules," *Proc. Japan Natl. Heat Trans. Symp*., (1995), 829-830.

[5] Maruyama, S., Kurashige, T., Matsumoto, S., Yamaguchi, Y. and Kimura, T., "Liquid Droplet in Contact with a Solid Surface," *Micro. Thermophys. Eng.*, **2**-1 (1998), 49-62.

[6] Kimura, T. and Maruyama, S., "Molecular Dynamics Simulation of Nucleation of Liquid Droplet on Solid Surface," *Therm. Sci. Eng.*, **8**-5 (2000), 7-13 in Japanese.

[7] Kimura, T. and Maruyama, S., "A Molecular Dynamics Simulation of Heterogeneous Nucleation of a Liquid Droplet on Solid Surface," *Micro. Thermophys. Eng.*, **6**-1 (2002), 3-13.

[8] Maruyama, S. and Kimura, T., "A Molecular Dynamics Simulation of a Bubble Nucleation on Solid Surface," *Int. J. Heat & Technology*, **18** (2000), 69-74.

[9] Maruyama, S. and Kimura, T., "A Molecular Dynamics Simulation of Bubble Nucleation on Solid Surface," *Trans. JSME (Ser. B)*, **65**-638 (1999), 3461-3467 in Japanese.

[10] Maruyama, S. and Kimura, T., "A Study on Thermal Resistance over a Solid-Liquid Interface by the Molecular Dynamics Method," *Therm. Sci. Eng.*, **7**-1 (1999), 63-68.

[11] Kandlikar, S. G., Maruyama, S., Steinke, M. E. and Kimura, T., "Measurement and Molecular Dynamics Simulation of Contact Angle of Water Droplet on a Platinum Surface," *HTD (Proc. ASME Heat Transfer Division 2001)*, **369**-1 (2001), 343-348.

[12] Kimura, T. and Maruyama, S., "Molecular dynamics simulation of water droplet in contact with platinum surface," *Proc. 12th Int. Heat Transfer Conf.*, (2002), 537-542.

[13] Israelachvili, J. N., *Intermolecular and Surface Forces*, Academic Press, London, (1985).

[14] Berendsen, H. J. C., Grigera, J. R., and Straatsma, T. P., “The Missing Term in Effective Pair Potentials”, *J. Phys. Chem.*, **91**-24 (1987), 6269-6271.

[15] Tully, J. C., “Dynamics of Gas-surface Interactions: 3D Generalized Langevin Model Applied to fcc and bcc Surface”, *J. Chem. Phys.*, **73**-4 (1980), 1975-1985.

[16] Blömer, J., and Beylich, A. E., “Molecular Dynamics Simulation of Energy Accommodation of Internal and Translational Degrees of Freedom at Gas-Surface Interfaces”, *Surf. Sci.*, **423** (1999), 127-133.

[17] Holloway, S., and Bennemann, K. H., “Study of Water Adsorption on Metal Surfaces”, *Surf. Sci.*, **101** (1980), 327-333.

[18] Spohr, E., and Heinzinger, K., “A Molecular Dynamics Study on the Water/Metal Interfacial Potential”, *Ber. Bunsenges. Phys. Chem.*, **92** (1988), 1358-1363.

[19] Zhu, S.-B., and Philpott, M. R., “Interaction of Water with Metal Surfaces”, *J. Chem. Phys.*, **100**-9 (1994), 6961-6968.